

Design, Optimization, and Control of a New Class of Reconfigurable Hopping Rovers

Chris Schmidt-Wetekam, David Zhang, Robert Hughes and Thomas Bewley

Flow Control and Coordinated Robotics Labs, UC San Diego

{cmschmid, dzhang, rphughes, bewley}@ucsd.edu

Abstract—A patent-pending new class of reconfigurable battery-powered hopping rovers for reconnaissance, exploration, defense, homeland security, and entertainment applications is publicly presented for the first time. A time-periodic linear quadratic regulator for stabilization of hopping maneuvers is presented, with simulation results. Additionally, a novel mechanical design for efficient and multi-modal operation is discussed, including a lockable hopping mechanism for the directed release of gradually accumulated elastic energy, utilizing two coupled four-bar linkages in tandem with a quick-release spring device.

I. INTRODUCTION

The balancing of an inverted pendulum on a moving cart has been a (perhaps, *the*) canonical control problem in academia for decades. The system sparks broad interest because, near the upright equilibrium, the system is unstable, under-actuated, and non-minimum phase; many similar stabilization problems exist in industry, such as the control of a rocket via gimbaling of the nozzle. Further, swinging from the (stable) hanging equilibrium to catch the system at the (unstable) upright equilibrium is a difficult trajectory optimization problem in which the system experiences challenging nonlinearities; similar trajectory optimization problems also exist in industry, such as the efficient and accurate launching of a satellite into orbit.

Both the stabilization of the pendulum system near the upright equilibrium and the swinging up of this system from the hanging equilibrium have been accomplished with a wide variety of techniques in the controls literature. As a challenging demonstration problem, our lab has used the adjoint-based Model Predictive Dynamic OPTimization (MPDopt) toolbox which we have developed at UCSD, not simply to swing up a single pendulum, but to simultaneously swing up two pendula of different lengths hanging from the same cart. A video of this result, together with an open-source version of the easily-extensible MPDopt code used to obtain it, is available at <http://renaissance.ucsd.edu/MPDopt>.

The next natural step with such systems is to eliminate the track, rolling the cart on the floor on its own wheels, under its own power, with all control electronics mounted onboard. In fact, the Segway Human Transport implements the solution to just such a problem; the novelty of this solution is that the control is implemented in such a manner as to move and balance in response a human standing on the cart.

This work is supported by the Los Alamos National Laboratory.



Fig. 1. Reconfigurable hopping rover capabilities. Note that the transition between horizontal and upright roving modes is achieved via a control sequence solved for using an adjoint-based optimization on the non-smooth rover dynamics [1]

Inspired by such technologies, our lab set out to explore what could be accomplished with an *autonomous*, self-contained inverted pendulum configuration. In most useful applications, such a system would need the capability to right itself from horizontal, and in many applications an efficient and simple mechanism to get past simple obstacles that could not be rolled over would be necessary. This realization has inspired the creation of a reconfigurable wheeled rover with hopping capabilities (Fig. 2).

Prior work on hopping robots has focused on designs in which an extendable leg is pivoted about a 2-DOF hip attached to the main robot body ([3] and [4]). A fusion of such designs with wheeled locomotion has resulted a patent-pending new class of battery-powered hopping rovers. These rovers utilize two main drive wheels with tank-style steering, in conjunction with a third orthogonal wheel and a spring loaded hopping mechanism, in order to re-orient the vehicle during flight using reaction torque. In this regard, the wheels on our robot act as legs with unlimited rotation. Eliminating the finite angular displacement of a hip joint allows our vehicle to make significant attitude corrections during flight, as well as to balance on its foot in three dimensions, or even perform running jumps, as illustrated in Fig. 1.

This design is characterized by high maneuverability, such as that normally associated with a unicycle. It may also be miniaturized significantly, making mass production



Fig. 2. Reconfigurable wheeled rover with hopping capabilities.

at reasonable cost viable. Ultimately, numerous potential markets for this class of robots are envisioned, ranging from the toy market to defense, homeland security, fire/rescue, nuclear waste monitoring, and scientific exploration.

II. TIME-PERIODIC CONTROL OF CONTINUOUS HOPPING

The difficulty in controlling hopping systems lies in the fact that the governing equations of motion are discontinuous and nonlinear. Nevertheless, such a system has been successfully stabilized via a strategy that combines three decoupled controllers: (1) an inner loop controller for re-orienting the body during flight, (2) a tabular leg placement algorithm based on the takeoff state and desired horizontal (running) velocity, and (3) a hopping height controller ([3]). The main drawback of this approach is the memory required to store tabular data sufficient for all possible operating conditions. In this section we derive and present simulation results of Linear Time-Periodic (LTP) Quadratic Regulator that stabilizes the full discontinuous, nonlinear dynamics under conditions for which the vehicle is nearly aligned with its pre-impact velocity during landings.

A. Equations of Motion

The key to developing a successful controller has been constructing linear equations of motion that recreate the discontinuous momentum exchange associated with landing impacts. (Fig. 3).

Specifically, the robot tips sideways after landing, if the line connecting the center of mass and point of ground

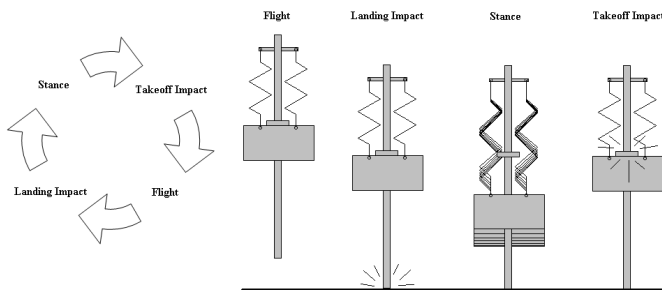


Fig. 3. Four unique phases of hopping motion. Note that the landing and takeoff innpacts are unique, since the horizontal velocity of the foot is not necessarily stationary before landing.

contact is not tangent to the pre-impact velocity. This transverse forcing brings to mind the familiar problem of an inverted pendulum with externally applied horizontal disturbances. Therefore, let us model the hopping robot as an extendable inverted pendulum with periodic transverse forcing affected by the conversion of linear momentum into angular momentum as the no-slip condition is enforced upon landing. Accordingly, consider an idealized planar model of hopping motion, in which the robot leg and body behave as a single mass, m , with rotational inertia, J , attached to a time-varying massless spring/damper that slides horizontally along a fictitious slot (Fig. 4).

Applying Lagrange's equations to this system, including forces applied by motorized reaction wheels and the hopping propulsion mechanism (omitted in preceding figures for clarity), yields the following nonlinear equations of motion,

$$\begin{bmatrix} J + mr_{bg}^2 & 0 & -mr_{bg} \cos \theta & 0 \\ 0 & m & -m \sin \theta & 0 \\ -mr_{bg} \cos \theta & -m \sin \theta & m & 0 \\ 0 & 0 & 0 & J_w \end{bmatrix} \begin{bmatrix} \ddot{\theta} \\ \ddot{r}_{bg} \\ \dot{x}_g \\ \dot{\phi} \end{bmatrix} = R,$$

where

$$R = \begin{bmatrix} mr_{bg}g \sin \theta - 2mr_{bg}\dot{r}_{bg}\dot{\theta} + N[b_{em}(\dot{\phi} - \dot{\theta}) - su(t)] - b_{ap}\dot{\theta} \\ mr_{bg}\dot{\theta}^2 - mg \cos \theta - k(t)(r_{bg} - r_0) + P + S(t)u_h(t) - B_{em}(t)\dot{r}_{bg} \\ 2m\dot{r}_{bg}\dot{\theta} \cos \theta - mr_{bg}\dot{\theta}^2 \sin \theta - b_x(t)\dot{x}_g \\ b_{em}(\dot{\theta} - \dot{\phi}) + su(t) - b_{aw}\dot{\phi} \end{bmatrix}.$$

Note that ϕ denotes the angular position of the reaction wheel(s) w.r.t. an inertial reference frame, and $u(t)$, $u_h(t)$ denote the control input into the reaction wheels and hopping motor, respectively. The system parameters are given in Tab.I, where $b_{em} \equiv \frac{\gamma k_{rv}}{R} + b_{friction}$, and $B_{em}(t) \equiv \frac{(GK_t)^2}{R_h} + b_i(t)$.

This single model encompasses all four phases of hopping motion, including finite-duration impacts, through the use of time-varying springs and dampers. During takeoff, landing

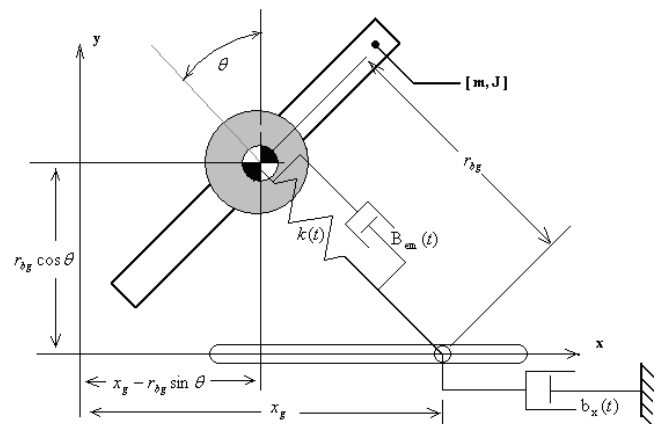


Fig. 4. Planar mass-spring-damper model of hopping motion. The time-varying spring/damper assembly, $k(t)/B_{em}(t)$, represents the robot leg, and is set to zero during flight. Time-varying horizontal damping, $b_x(t)$, simulates the no-slip condition during stance.

Parameter	Category	Description
g		Gravity
m	Robot Body	Total robot mass
J		Moment of inertia
b_{ap}		Air drag damping
J_w	Reaction Wheels	Moment of inertia
b_{aw}		Air drag damping
N		Wheels per axis
k_t	Reaction Wheel Motors	Torque constant
γ		Gear reduction
v		Supply voltage
R		Terminal resistance
$s \equiv \frac{\gamma k_t v}{R}$		Stall Torque
b_{em}		Damping coefficient
$k(t)$		Spring constant
r_0	Hopping Mechanism	Takeoff/landing height
P		Spring pre-tension
ρ		Pinion gear radius
K_t	Hopping Motor	Torque constant
G		Gear Reduction
V		Supply Voltage
R_h		Terminal resistance
$S \equiv \frac{GK_t V}{\rho R_h}$		Stall force at supply voltage
$b_i(t)$	Radial Dynamics	Time-varying takeoff impact dissipation coefficient
$B_{em}(t)$		Damping coefficient
$b_x(t)$	No Slip Condition	Damping coefficient

TABLE I
PARAMETERS OF IDEALIZED HOPPING MODEL

and stance, the no-slip condition between the foot and ground is modeled via large horizontal damping at the foot, $b_x(t)$, which may modulated depending on the available traction. Similarly, the energy loss associated with impacts between the body and leg on takeoff is modeled by applying large radial damping on the body during a finite takeoff impact period, as represented by the time-varying damper, $B_{em}(t)$. Lastly, during flight, all spring and damping terms are set to zero, such that the robot rotates about its center of mass. It is assumed that both the pitch and roll dynamics of the actual six degree of freedom system may be modeled using decoupled planar dynamics of this form, provided that the angles and angular velocities of the system remain small.

Linearizing these equations about the unstable equilibrium yields the LTP state space system,

$$E(t)\dot{\mathbf{x}} = \bar{A}(t)\mathbf{x} + \bar{B}\mathbf{u},$$

where

$$E = \begin{bmatrix} J + mr_{bg}(t)^2 & 2mr_{bg}(t)\dot{r}_{bg}(t) & -mr_{bg}(t) & 0 & 0 \\ 0 & 1 & 0 & 0 & 0 \\ -mr_{bg}(t) & -2m\dot{r}_{bg}(t) & m & 0 & 0 \\ 0 & 0 & 0 & 1 & 0 \\ 0 & 0 & 0 & 0 & J_w \end{bmatrix},$$

$$\bar{A} = \begin{bmatrix} -Nb_{em} - b_{ap} & mgr_{bg}(t) & 0 & 0 & Nb_{em} \\ 1 & 0 & 0 & 0 & 0 \\ 0 & m\dot{r}_{bg}(t) & -b_x(t) & 0 & 0 \\ 0 & 0 & 1 & 0 & 0 \\ b_{em} & 0 & 0 & 0 & -b_{em} - b_{aw} \end{bmatrix},$$

$$\bar{B} = [-Ns \quad 0 \quad 0 \quad 0 \quad s]^T,$$

and

$$\mathbf{x} = [\ddot{\theta} \quad \dot{\theta} \quad \ddot{x}_g \quad \dot{x}_g \quad \ddot{\phi}]^T.$$

Which may be rewritten in the form

$$\dot{\mathbf{x}} = A(t)\mathbf{x} + B(t)\mathbf{u},$$

where $A(t)$ and $B(t)$ are piecewise continuous matrices

$$A(t) = E^{-1}(t)\bar{A}(t),$$

and

$$B(t) = E^{-1}\bar{B}(t).$$

Note that the radial trajectory, $[\dot{r}_{bg}(t), r_{bg}(t), r_{bg}(t)]^T$, enters the linearized system as time-periodic parameters in the E and A matrices, due to the assumption that these dynamics are almost completely decoupled from the rest of the system. As verified in simulation, this simplification is valid as long as the center of mass and the point of ground contact lie nearly along the line tangent to the pre-impact velocity, which is the type of motion expected of a stably hopping robot.

B. Differential Riccati Equation

Suppose we wish to minimize the following measure of system behavior,

$$J \equiv \int_0^{\infty} (\mathbf{x}^* Q \mathbf{x} + \mathbf{u}^* R \mathbf{u}) dt,$$

which may be interpreted as a summation of the state variance, and control input energy over an infinite time horizon. It can be shown that the linear control law that minimizes J is given by

$$K(t) = -R^{-1}B(t)^*X(t),$$

where $X(t) > 0$ is obtained by marching the Differential Riccati Equation (DRE) backwards in time

$$-\dot{X}(t) = A(t)^*X(t) + X(t)A(t) - X(t)B(t)R^{-1}B(t)^*X(t) + Q.$$

As shown in Fig. 5, for our particular system, the control

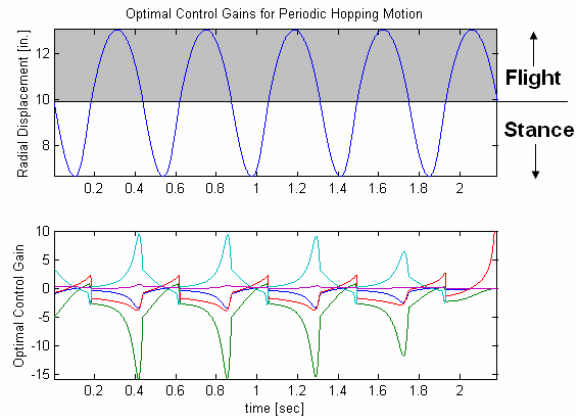


Fig. 5. Convergence of time-varying control gains to a periodic solution using Runge-Kutta 4 (RK4). An algorithm leveraging the cyclic QZ decomposition may also be used to solve the periodic Riccati equation [2].

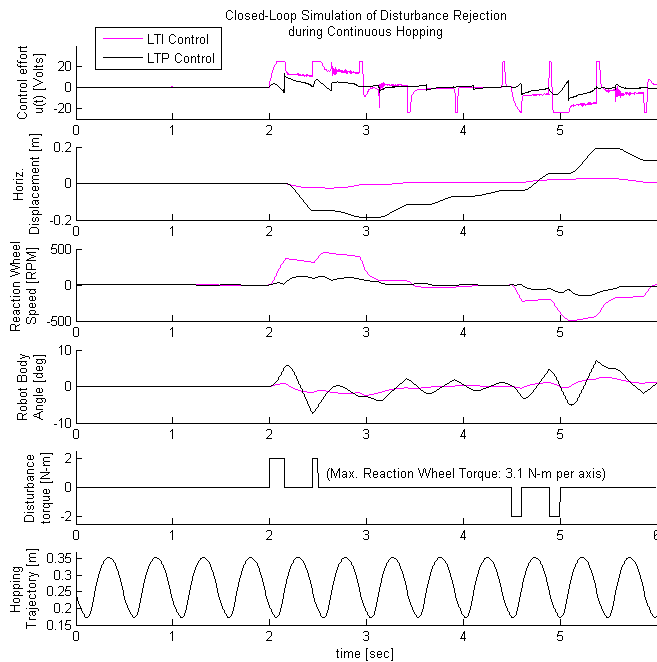


Fig. 6. Closed-loop simulation of disturbance rejection using time-periodic gains on the nonlinear plant model.

gains converge to a periodic solution after approximately 2 periods. Note that the control gains peak before each landing. This is particularly interesting, as these spikes precede, rather than track, system dynamics discontinuities associated with landing impact.

Intuitively, the resulting periodic gains reflect the increased control authority available during flight, due to both the reduced rotational inertia, and the absence of a normal ground force opposing gravity. Therefore, the periodic controller leverages these time-varying dynamics by manipulating the takeoff angle and angular orientation during flight, such that the misalignment between the robot and its ballistic trajectory upon landing induces a moment that simultaneously stabilizes the angular orientation and counteracts the motor-torque necessary to bleed off reaction wheel speed. Namely, the controller augments the reaction wheel torque by appropriately converting radial momentum into angular momentum on landing.

As shown in Fig. 6, linear time-periodic control attenuates disturbances using far less control effort than LTI control; note that, for LTI control $\int_0^T u^2 dt = 0.62$, compared to $\int_0^T u^2 dt = 0.037$ for LTP control (T is the elapsed simulation time). Although LTI control produces less angular orientation variance, this comes at the expense of greatly increased control effort, which counters the objective of maximum disturbance rejection. Furthermore, the horizontal trajectory is uncontrollable via LTI controllers, since the system is fixed to the ground during stance, and unable to affect its linear momentum during flight, therefore an LTP controller is necessary to achieve forward/backward hopping motion.

Future work will investigate the use of gain scheduling

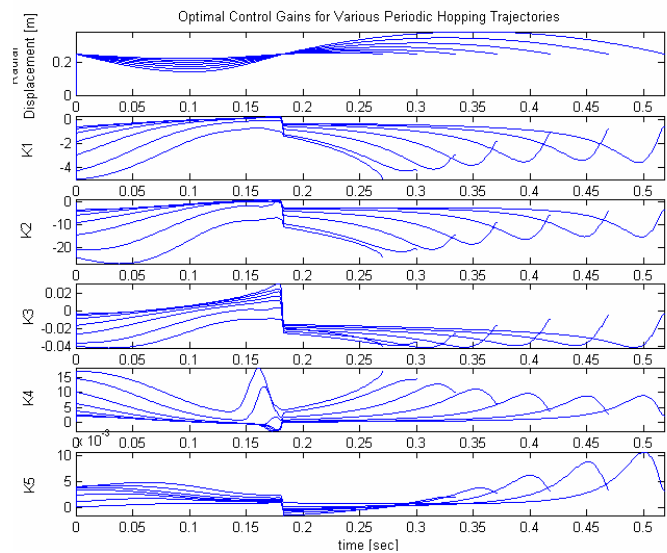


Fig. 7. Breadth of optimal LTP control gains over anticipated hopping trajectories.

between a pre-computed set of LTP control sequences (Fig. 7) in order to facilitate the control of continuous hopping on uneven surfaces. Such developments, in addition to refinements in state estimation, are requisite to the implementation of LTP control on the physical prototype.

III. DESIGN AND OPTIMIZATION OF PHYSICAL PROTOTYPE

The philosophy throughout the physical design process has been to minimize weight, cost and complexity (and hence maximize control authority) by adapting components to perform multiple functions. To this end, the drive wheels propel and steer the vehicle as a rover, as well as re-orient the vehicle between each hop. Additionally, the hopping propulsion mechanism utilizes two coupled 4-bar linkages that 1) produce linear motion, 2) behave as a continuously variable transmission (CVT), and 3) can be locked into and out of a highly tensioned state, facilitating off-line accumulation of hopping energy using low-power actuators.

A. Reaction Wheel Design

When out of contact with the ground, the wheels re-orient the robot by conservation of angular momentum; i.e. the reaction wheels sacrifice their orientation for the sake of body and leg. The torque-speed curve of the reaction wheel motors creates an incentive for heavy reaction wheels, as this maximizes operation of the wheel-motors in a high-torque/low-speed state. Even for the largest wheels that fit within the robot's packaging constraints, a significant amount of ballast (approx. 10% of the total robot mass) must be added to each wheel, in order to create sufficient moment of inertia for effective disturbance rejection. Yet, this added mass amplifies destabilizing ground normal forces, which, in turn, necessitates larger, more powerful reaction wheel motors. The obvious solution to this "catch twenty-two" has

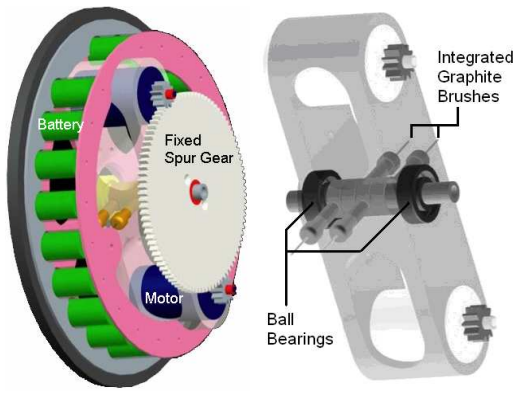


Fig. 8. Integrated reaction wheel design. Two drive motors near the wheel perimeter engage a concentric spur-gear fixed to the robot body. Battery cells mounted around the circumference power the motors, and pass current to the robot body via integrated graphite brushes.

been mounting "live weight" (i.e. the motors and batteries) along the circumference of the reaction wheel itself (Fig. 8).

Compared to a conventional motor with a miniature multi-stage gearbox, this design can transmit significantly more torque with fewer losses, while reducing radial loading of the motor output shafts, and providing air-cooling of the motors.

B. Hopping Propulsion Mechanism

The development of a spring-loaded dual four-bar linkage has facilitated the directed release of gradually accumulated elastic energy using low-power DC gearmotors. This design was motivated by the desire to continuously vary the torque/speed relationship between the hopping actuator and the leg; i.e. high-speed/low-torque operation during takeoff/landing and low-speed/high-torque operation during each rebound. Other novel hopping mechanisms have also served as inspirations for this design [4], [5], and [6].

An intuitive way of implementing such a gear reduction would be via a conical spool-and-wire drive (Fig. 9). A similar effect has been achieved through a combination of two four-bar linkages, with the added benefit of linear motion and locking capability (Fig. 10). The linkage kinematics

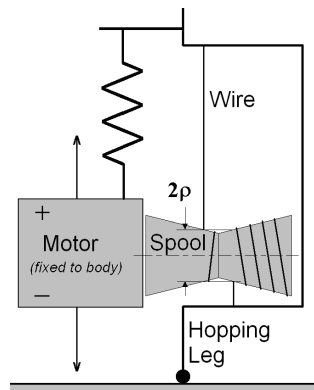


Fig. 9. spool and dual-wire drive concept. Spools would contain helical grooves to guide the wires.

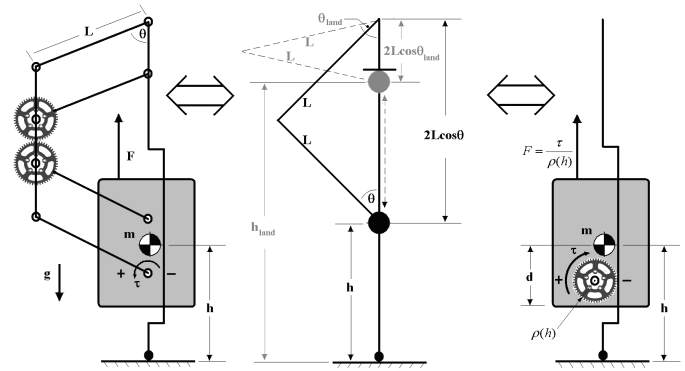


Fig. 10. Kinematics of four-bar hopping mechanism in terms of an analogous continuously variable rack & pinion gear-set with radius $\rho(h)$ (springs and spring forces omitted for clarity).

follow from basic geometry

$$\rho(h) = 2L \sin \theta = \sqrt{L^2 - \frac{(h_{land} + 2L \cos \theta_{land} - h)^2}{4}}$$

where h_{land} and θ_{land} denote the height of the robot center of mass, and linkage angle at takeoff/landing, respectively.

Given a four-bar linkage with a maximum stroke length, $h_{land} - d$, allowed by packaging constraints on the link-length, L , and a motor size limited by battery current-draw constraints, a good approximation of the optimal hopping motor gear ratio, G , is given by

$$G = \frac{E \sqrt{2g(h_{apex} - h_{land})}}{\omega_{pmax} \rho(L, h_{land}, \theta_{land})}$$

where h_{apex} is the anticipated fully-developed hopping height, g is the gravitational constant, E is the coefficient of restitution associated with takeoff impact, and ω_{pmax} is the velocity of the hopping motor at peak power output.

Continuous hopping performance is maximized by using the softest spring capable of preventing the robot from "bottoming out", as this maximizes both the duration of stance-phase energy injection, and the spring energy storage capacity for a given peak spring tension. Namely, the optimal spring constant is given by

$$k = \frac{2mg(h_{apex} - h_{land})}{h_{land} - d}$$

Given these parameters, the performance gains of the dual four-bar mechanism over a fixed ratio rack & pinion drive is demonstrated in simulation (Fig. 11). Note the smoothing of the motor shaft speed, ω , near the fully-tensioned state, and the corresponding increases in linear force, F , transmitted from the body onto the leg, for the case of four-bar actuation.

The continuously variable torque-speed characteristics of the four-bar mechanism are complemented by the ability of this mechanism to function as a locking quick release, even under extreme tension. Namely, since the effective gear ratio between the hopping motor and dual four-bar linkage is infinite at $\theta = 0^\circ$, the hopping mechanism drive motor is

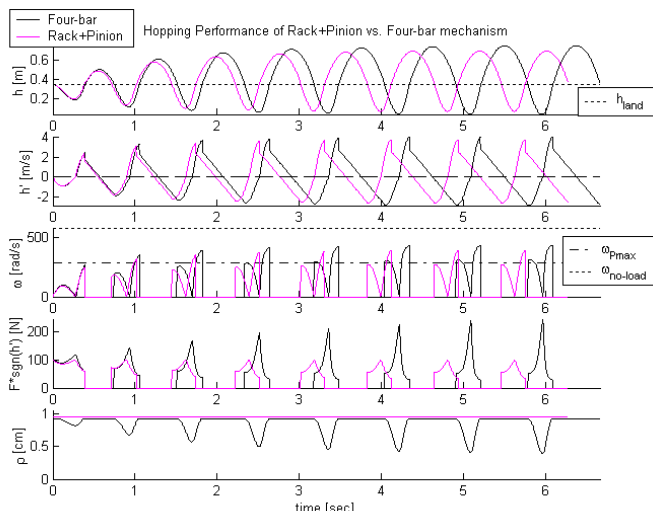


Fig. 11. Comparison of purely vertical hopping performance of rack-and-pinion vs. four-bar drive mechanisms, given $L = .17m$, $G = 30 : 1$, $\theta_{land} = 90^\circ$, $h_{land} = .35m$.

capable locking the robot leg into and out of a fully tensioned state while roving (Fig. 12).

By pre-tensioning the springs during this locked state, the mechanism may initiate single large hops and even running jumps from and immediately back into upright roving mode, as illustrated in Fig. 1. This locking capability facilitates efficient jumping maneuvers by eliminating the requirement for real-time injection of hopping energy; i.e. energy may be gradually accumulated in the springs *before* release, using a low-power, high-torque lead-screw spring tensioner.

The single hop capability also has the distinct advantage of maximizing operation of the robot in the highly controllable, and efficient upright roving mode. This capability will be

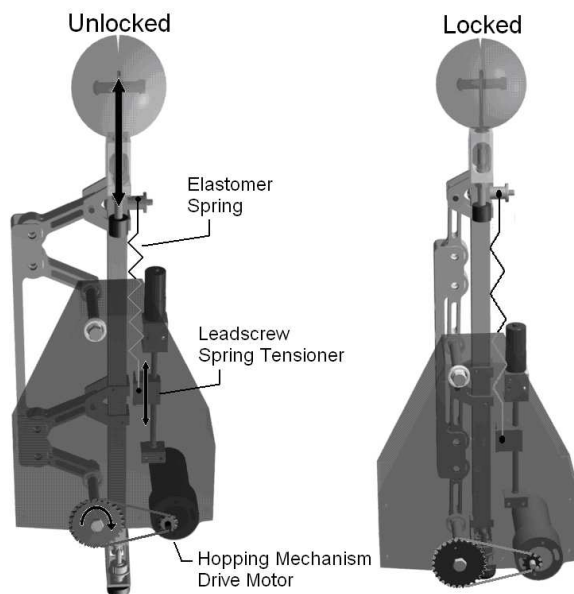


Fig. 12. CAD rendering of hopping mechanism in both locked and unlocked states.

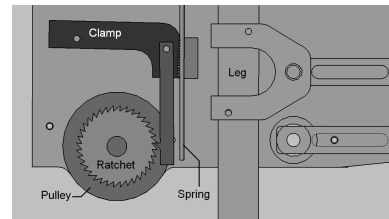


Fig. 13. CAD rendering of quick-release spring clamping concept.

leveraged in order to efficiently and robustly climb stairs. Namely, the robot begins on a bottom step in upright roving mode with the four-bar locked in tension, launches itself upward by releasing this tension, and immediately reverts back into upright roving mode upon reaching the next step, by reversing the hopping mechanism drive motor on landing. This process will be facilitated by the development of a spring tensioning mechanism that is able to quick release (Fig. 13), as the current prototype relies partly on momentum in order to lock back into a tensioned state.

IV. CONCLUSIONS/FUTURE WORK

The mechanical design and control strategy for a new class of hopping rovers has been presented. These innovations have led to a unique fusion of hopping and rolling motions, coordinated by time-periodic LQR and adjoint-based optimal trajectory planning. In contrast to the MIT [3] and Carnegie-Mellon [4] hoppers, optimal control is used to stabilize and coordinate stationary and running hopping motions, with the additional capability of righting the robot from rest on the ground.

Future development of the rover will focus on object recognition, spatial awareness, stair-climbing, and object manipulation. On-board vision systems, coupled with extended kalman filtering of inertial measurements will facilitate the development of fully-autonomous variants of the current prototype. Furthermore, the manipulation of objects (for instance the retrieval and tossing of balls for entertainment and sport) is another exciting application suited for such a dynamic platform. These prospects, combined with the inherently fascinating aspects of hopping robots, promise to make this an exciting field of research for years to come.

REFERENCES

- [1] S. Summers, & T.R. Bewley, "Adjoint Based Trajectory Planning for a Multi-Functional & Reconfigurable Robotic Ground Vehicle". Proceedings, 7th Conference on Mobile Robots and Competitions (CDC2007); April 27, 2007.
- [2] J. J. Hench, & A. J. Laub, "Numerical Solution of the Discrete-Time Periodic Riccati Equation." IEEE Transaction on automatic control, vol. 39, No. 36, June 1994.
- [3] Marc H. Raibert, *Legged Robots that Balance*. The MIT Press series in artificial intelligence. Cambridge, Massachusetts. 1986.
- [4] H. Brown, & G. Zeglin, "The Bow Leg Hopping Robot." IEEE International Conference on Robotics and Automation, 1998.
- [5] K.V. Papantoniou, "Electromechanical design for an electrically powered, actively balanced one leg planar robot." IEEE/RSJ International Workshop on Intelligent Robots and Systems, 3, 1553-60, 1991.
- [6] N. Delson; T. Hanak; K. Loewke; D.N. Miller, "Modeling and implementation of McKibben actuators for a hopping robot." Proceedings, 12th International Conference on Advanced Robotics July 18-20, 2005 Pg:833 - 840